

Using wetting and ultrasonic waves to extract oil from oil/water mixtures

Yifan Li,[†] J. M. Marcos,[‡] Mark Fasano,[¶] Javier Diez,[§] Linda J. Cummings,[¶] Lou Kondic,[¶] and Ofer Manor^{*,†}

[†]*The Wolfson Faculty Department of Chemical Engineering, Technion — Israel Institute of Technology, Haifa 3200003, Israel*

[‡]*Departamento de Física, Universidad de Extremadura, 06006 Badajoz, Spain*

[¶]*Department of Mathematical Sciences, New Jersey Institute of Technology, Newark, New Jersey 07102, USA*

[§]*Instituto de Física Arroyo Seco, Universidad Nacional del Centro de la Provincia de Buenos Aires, and CIFICEN-CONICET-CICPBA, Pinto 399, 7000, Tandil, Argentina*

E-mail: manoro@technion.ac.il

Abstract

Oil and water phases placed on top of a solid surface respond differently to a MHz-level surface acoustic wave (SAW) propagating in the solid due to their different surface tensions and the corresponding capillary stresses. We observe that, under SAW excitation, oil films are extracted continuously from sessile drops of silicone-oil/water/surfactant mixtures. The mechanism responsible for the extraction of oil from the mixtures is the *acoustowetting* phenomenon: the low surface tension oil phase leaves the mixture in the form of ‘fingers’ that initially spread over the solid in the direction transverse to that of the SAW. Once away from the drop the oil spreads on the solid surface in the direction opposite that of the SAW, as in classic studies on

acoustowetting. The high surface tension water phase remains at rest. Increasing the SAW intensity and oil content in the mixtures enhances the rate at which oil leaves the emulsion. We further observe that the oil film develops free surface instabilities in the form of periodic spatial variations, as well as the formation of spatial gradients in the emulsion concentrations in the presence of SAW. Our study suggests the potential for using SAW to remove oil from oil-in-water mixtures to facilitate the small-scale separation of water and oil phases. Furthermore, we describe the peculiar physical effects leading to acoustic-capillary flow instabilities and SAW-induced emulsion dynamics.

Introduction

One of the principal contributions to shortages in drinking water is the use and pollution of water by industry, e.g., pharmaceutical and healthcare emulsion processing¹ and petroleum extraction,²⁻⁴ oil extraction in the food industry,^{5,6} and domestic processes that produce gray water.⁷ A key process when reclaiming water is the separation of oily liquids from the water body. The established techniques for separating oil from water require extensive energy investment and add-on chemicals. At the large scale, this means employing high power distillation⁸ or chemicals to force coagulation/flocculation of oil droplets.^{9,10} These methodologies have been used for approximately two hundred years and are compatible with large-scale water recovery facilities. Micro-scale setups for breaking oil-in-water emulsions down to their constituent phases are preferable to existing macro-scale emulsion-breaking methods for the local recovery of gray water in domestic housing and small-scale industrial applications. Here, we explore the interplay between capillary and acoustic stress in oil-in-water mixtures for small-scale phase separations.

It was recently discovered that MHz-frequency SAWs, traveling along the surface of a solid substrate, generate different responses in oil and water. Initial studies concentrated on silicone oil; in particular, Rezk et al.¹¹⁻¹³ excited a drop of silicone oil on the horizontal substrate of SAW actuators and observed that an oil film emanates from the drop and

dynamically wets (spreads over) the solid in the direction opposing that of the traveling SAW, a phenomenon that has been called *acoustowetting*. The wetting rate of the oil films correlates with the oil viscosity; with the SAW intensity, ωA , where A is the normal displacement amplitude induced by the SAW at the solid surface and ω is the angular frequency of the SAW; and with the film thickness, H , which was measured to be tens of micrometers in magnitude (the exact value is determined by a balance between acoustic and capillary stresses). Moreover, Collins et al.¹⁴ and Manor et al.¹³ suggest specific stable values for the film thickness H , that correlate with the wavelength of ultrasound leakage off the SAW. In particular, for a silicone oil of a 20 mN/m surface tension excited by a 20 MHz SAW, H was measured to be $H \approx 20 \mu\text{m}$, regardless of the acoustic power.^{11,12}

Altshuler et al.^{15,16} further considered the case of partially wetting (finite three-phase contact angle) solutions of water and surfactants. They show that the acoustowetting phenomenon is the product of a balance between capillary and acoustic stresses in the liquid film. Capillary stress resists the formation and spreading of the films on the solid, while acoustic stress drives these effects. Altshuler et al.^{15,16} suggest that the dynamic wetting (spreading) of liquid films under the action of SAW is governed by the parameter θ^3/We , where θ is the three-phase contact angle between the liquid, vapor, and solid substrate, measured in radians, and $\text{We} \equiv \rho(\omega A)^2 H/\gamma$ is an ‘acoustic’ Weber number wherein ρ is the liquid density and γ is the surface tension at the oil-vapor interface. This parameter measures the ratio between acoustic and capillary stresses in the liquid film: if $\theta^3/\text{We} > 1$, the film is governed by capillary stresses resulting in a static drop, while if $\theta^3/\text{We} < 1$, the film is governed by acoustic stresses, leading to evolving films. The theory is compatible with previous silicone oil experiments, in which oil films that completely wet the solid at equilibrium ($\theta \approx 0$) were found to spread over the solid in the range of SAW intensities studied. In the case of water films, Altshuler et al.^{15,16} have confirmed experimentally the validity of theoretical predictions, with the transition in the water film dynamics taking place at $\theta^3/\text{We} \approx 1$.

Horesh et al.¹⁷ further added gravity to disrupt the balance between acoustic and capillary

stresses and emphasize the differences in oil and water/surfactant solution response to SAW. The analysis was found useful for measuring acoustic stresses in partially wetting liquids: the authors found that silicone oil films were able to leave a reservoir and continuously climb up the surface of a vertical SAW actuator against gravity. However, water/surfactant solutions under the same conditions left the reservoir and climbed to a finite height of just a few millimeters up the same vertical SAW actuator. The finite height to which water/surfactant solutions climbed results from the competition between gravitational, capillary, and acoustic stresses in the climbing films.

In what follows, we use the differing responses of oil and water to SAW excitation to extract oil from a sessile drop of oil/water/surfactant mixtures. The silicone oil phase in the mixture, in the presence of a SAW with intensity in the range $\omega A \approx 1 - 1000$ mm/s commonly used for SAW microfluidics, satisfies the inequality $\theta^3/We \ll 1$ ($\theta \ll 1$ radians and $\gamma = 20$ mN/m), and the SAW induced acoustic stress in the liquid governs oil film dynamics. However, the water/surfactant phase ($\theta \approx \pi/6 - \pi/3$ radians ($30 - 60^\circ$) and $\gamma = 40 - 70$ mN/m) requires significantly higher SAW intensity (ωA) to render $\theta^3/We < 1$ and thus produce spreading. We experimentally use power levels below such values, therefore we may expect a different response of the silicone oil compared to that of the water or water/surfactant mixture. Exploration of these different responses of the emulsion components is our main focus.

The rest of this paper is structured as follows. The section *Experiment* describes our experimental procedure. In the subsequent section, *Formation and dynamics of oil films*, we discuss the oil film that leaves the emulsion drop. We then describe the temporal and spatial variations in the composition of the emulsion drops in *Variations in oil content in the emulsion drops*, and finally we give our further insights and perspective in *Conclusions*.

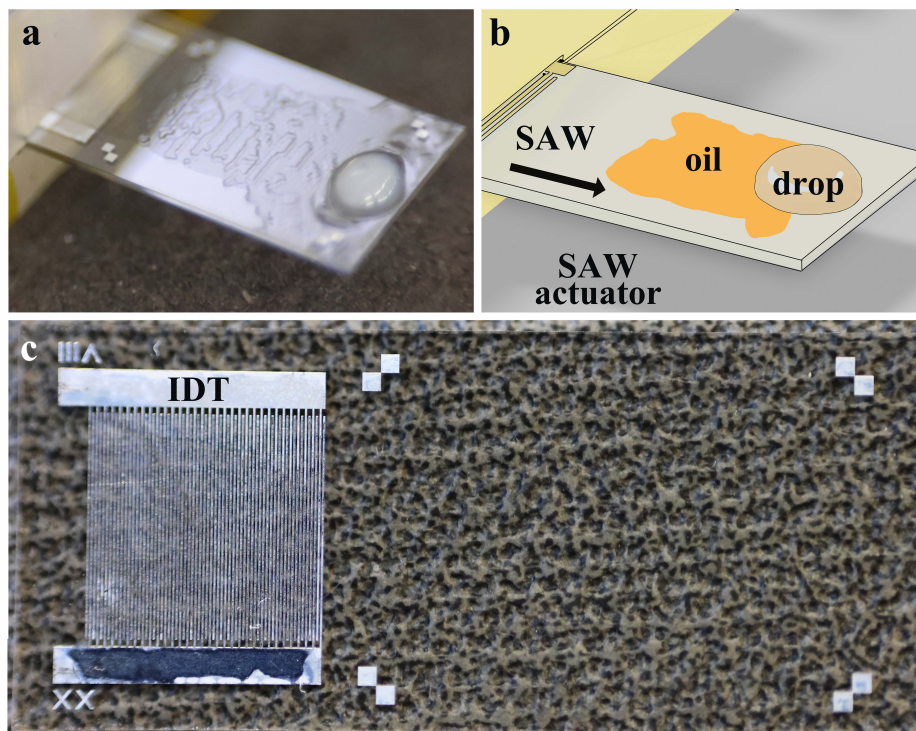


Figure 1: (a) Our experimental setup (view from above) where we position the SAW actuator that supports an emulsion drop using a 3D printed plastic case that connects the actuator to power and (b) a schematic sketch (view from above) of the same system, further illustrating the oil film emerging from the emulsion sessile drop under SAW excitation. (c) The SAW actuator (placed on a checkered surface) is comprised of inter-digital metal electrodes (referred to as IDT) fabricated on the top of a transparent piezoelectric lithium-niobate (LN) substrate; the sides of the metal squares fabricated atop the LN substrate, away from the IDT, are 0.5 mm long.

Experiment

We prepare surfactant—sodium dodecyl sulfate (SDS) and (separately) Tween 20—stabilized emulsions consisting of silicone oil droplets, approximately 230 nm in diameter (median drop size), in de-ionized water. Electrostatic and steric repulsion forces generated by the negatively charged surfactant, adsorbed on the emulsion droplets, counteract attractive van der Waals forces and support the emulsion’s kinetic stability. The drop size in the emulsion remains stable for 12 to 18 months when kept in a closed vessel on a lab shelf at approximately 20° C. No coalescence or creaming appears during this time, and the size of the emulsion droplets remains approximately the same; see further details in Supporting Information.¹⁸

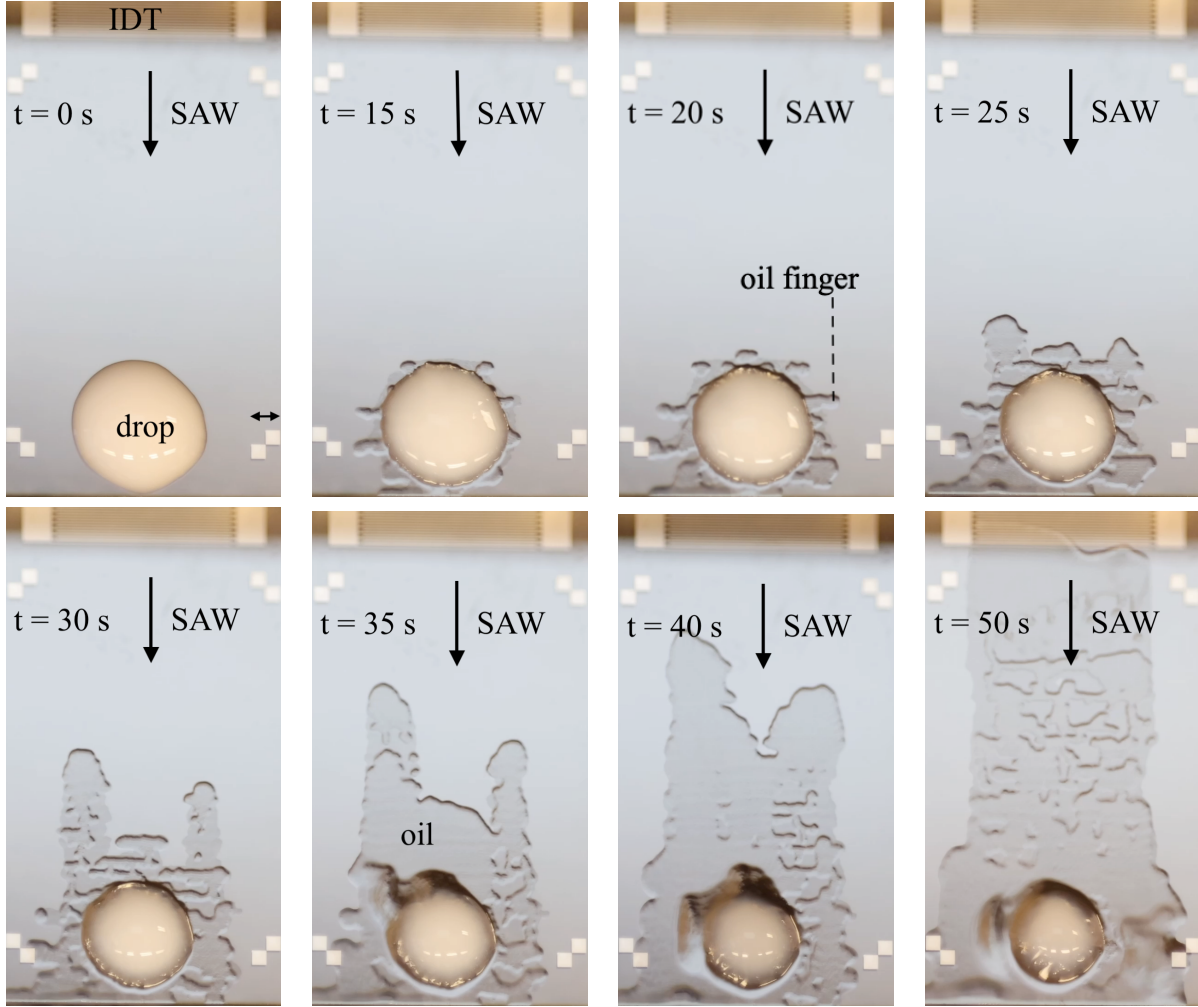


Figure 2: Top view of a typical experiment; in this and the following figures we use a $10 \mu\text{l}$ emulsion (40% oil-in-water emulsion, 230 nm oil droplets diameter) drop at lab ambient conditions (50% humidity, 20°C) if not specified differently. The SAW excitation amplitude is $A = 1.8 \text{ nm}$. Time $t = 0$ corresponds to the moment we observe the appearance of oil at the drop circumference, which here occurs after a wait-time period of $t_w = 190 \text{ s}$ after the commencement of SAW excitation. Initially ($t = 0 - 20 \text{ s}$), we observe that (transparent) fingers of oil leave the drop transverse to the path of the SAW. After $t = 20 \text{ s}$ the oil fingers that have emerged from the drop change direction and spread in the direction opposite the SAW propagation. At yet later times, the film of oil spreading between the emulsion drop and the electrodes on top of the SAW actuator (IDT) develops surface patterns characterized by a length scale of $\approx 0.5 \text{ mm}$. The double arrow in the $t = 0$ image is 1 mm long. Movies 1 and 2 in the Supplementary Information show both the top and side views of the experiment.

We place a drop of oil-in-water emulsion atop the solid substrate of an acoustic actuator and introduce a surface acoustic wave (SAW)—a Rayleigh wave of nanometer displacement amplitude—that travels in the solid substrate and comes in contact with the sessile drop. Figure 1 shows our experiment. The SAW is characterized by $\omega/2\pi = 20$ MHz-frequency and $200 \mu\text{m}$ wavelength that supports a surface normal displacement amplitude of $A = 0.5 - 2.5$ nm. These values of A correspond to a surface displacement velocity (particle velocity) of approximately $A\omega = 60 - 300$ mm/s in the direction normal to the solid surface. The SAW introduces excess acoustic stress in the neighboring fluid, with the consequence of extracting oil from the emulsion drop, as discussed next.

Figure 2 shows typical experimental results. The first three images of Figure 2 at $t = 0 - 20$ s show the initial time interval during which oil leaves the emulsion drop under SAW excitation. We observe an accumulation of transparent oil along the drop’s rim, followed by fingers of oil leaving the drop transverse to the path of the SAW (e.g., see the image at $t = 20$ s) and spreading over the solid substrate. We note that it is possible to distinguish between the emulsion and oil phases by color and wetting properties: the yellow milky color of the emulsion is a consequence of the diffraction of light by the emulsion nano-droplets. A transparent, clear, liquid suggests a pure or near-pure phase, either oil or water. Water and water/surfactant solutions on a lithium-niobate surface support a finite three-phase contact angle of^{15,16} $30 - 60^\circ$, while the low surface tension oil supports vanishing contact angle on the same substrate. Hence, a pure water/surfactant phase appears in the form of clear/milky drops, and a pure oil phase appears in the form of a clear liquid film, identifying the fingers that leave the drop as silicone oil. We speculate that the reason for oil finger formation (rather than a continuous film) is the limited availability of oil near the contact line of the drop. The initial evolution is followed at $t = 25 - 50$ s (the remaining images in Fig. 2) by a continuous oil film surrounding the drop and spreading over the solid substrate in the direction opposing the SAW. Moreover, for $t > 25$ s, the oil film away from the drop shows surface patterns due to variations in film thickness. Namely, the film thickness

undulates, forming hills and valleys, which are characterized by the in-plane length scale of approximately 0.5 mm; while we do not have at this point a good understanding of the source of such a lengthscale, we note that it is different from the 200 μm wavelength of the SAW.

Formation and dynamics of oil films

Figure 3 shows a side view of the emulsion drop, highlighting the initial formation of an oil film on top of the emulsion drop, which appears to be the source of the oil leaving the drop. Figure 4 compares an experiment exposed to the laboratory atmosphere of approximately 50% humidity and one in a humidity chamber that provides approximately 85% humidity; as we will see, quantifying the effect of humidity helps us understand the mechanism leading to the formation of oil film. The figure shows that the time taken for oil to leave the drop depends on the ambient humidity level, with the oil film emerging faster from emulsion drops at lower humidity, suggesting that evaporation plays a role.

Figure 5 further explores the effect of humidity as the intensity of the SAW is varied. We observe the general trend that the ‘waiting time’ t_w , (the time period between the start of SAW and the first appearance of the oil film) is shorter if humidity is lower. Consistent results were found when using different surfactants (as stated, two types were used: charged Sodium Dodecyl Sulfate (SDS) or non-charged (oily) polysorbate-type nonionic surfactant which includes 20 repeating units of polyethylene glycol (Tween-20)) to stabilize the emulsion. Similar formation of oil films during the evaporation of the water phase of oil/water mixtures is described elsewhere.^{19,20} It appears that the evaporation of the volatile water phase in the presence of the non-volatile oil phase renders the latter evermore concentrated in time until it forms a continuous film, which then leaves the drop. Figure 5 is also consistent with the expectation that an increase in humidity leads to a reduction in the water evaporation rate, and consequently an increase in the time required to form an oil film that could leave the

emulsion drop. Thus, both the rate of water evaporation and the level of SAW intensity influence the waiting time, t_w , at which oil leaves the emulsion drop.

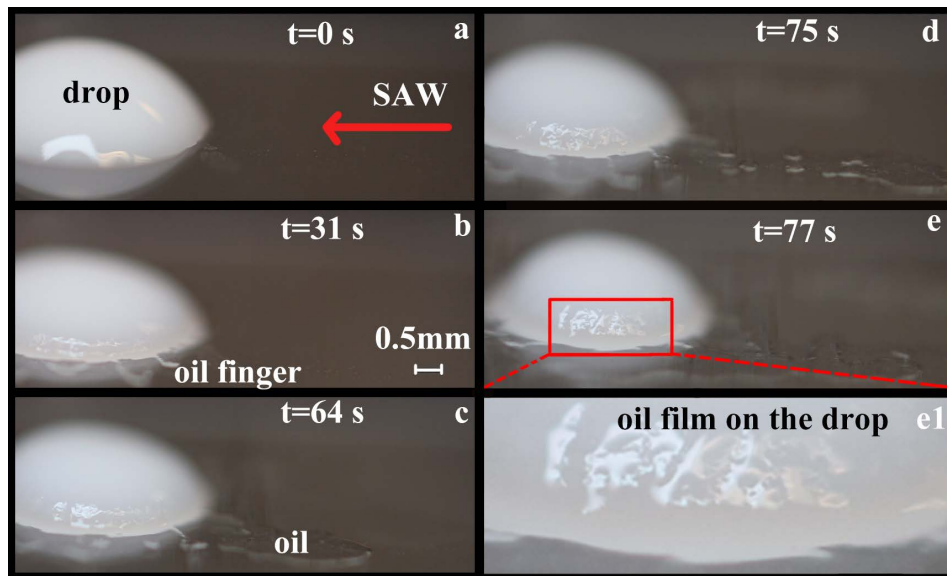


Figure 3: Side view time-lapse of an emulsion drop under the influence of SAW, where $t = 0$ gives the time at which oil appears at the drop circumference; the SAW excitation amplitude is $A = 1.8$ nm. Part a) Here, time $t = 0$ corresponds to $t_w = 150$ s from the commencement of SAW excitation. We observe the accumulation of an oil film atop the drop surface and along its rim. Part b) shows the initial formation of oil fingers leaving the drop; these oil fingers become longer as time progresses (as shown in parts c–e); the fingers merge at longer times to form a continuous oil film that spreads on the solid in the direction opposite to the SAW. See video #2 in Supplementary Information (SI).

Once oil films leave the drop, they spread on top of the solid substrate in the direction opposite that of the SAW. This motion suggests the *acoustowetting* effect, known to lead to such behavior in the case of oil films that originate from one-phase oil reservoirs, e.g., oil drops.^{11–13} In such one-phase oil systems the SAW leads to the formation and spreading of oil films of a thickness smaller than half the wavelength of the leaked ultrasonic waves that diffract off the SAW in the underlying solid substrate and propagate in the overlying fluid.

We employ 20 MHz-frequency SAW in our experiment, which leaks the same frequency ultrasound waves of approximately $80 \mu\text{m}$ wavelength. Hence, to verify our assertion about the acoustowetting phenomenon in our experiments, we proceed by measuring and discussing the thickness of the extracted oil film and show that it is indeed of a thickness smaller than

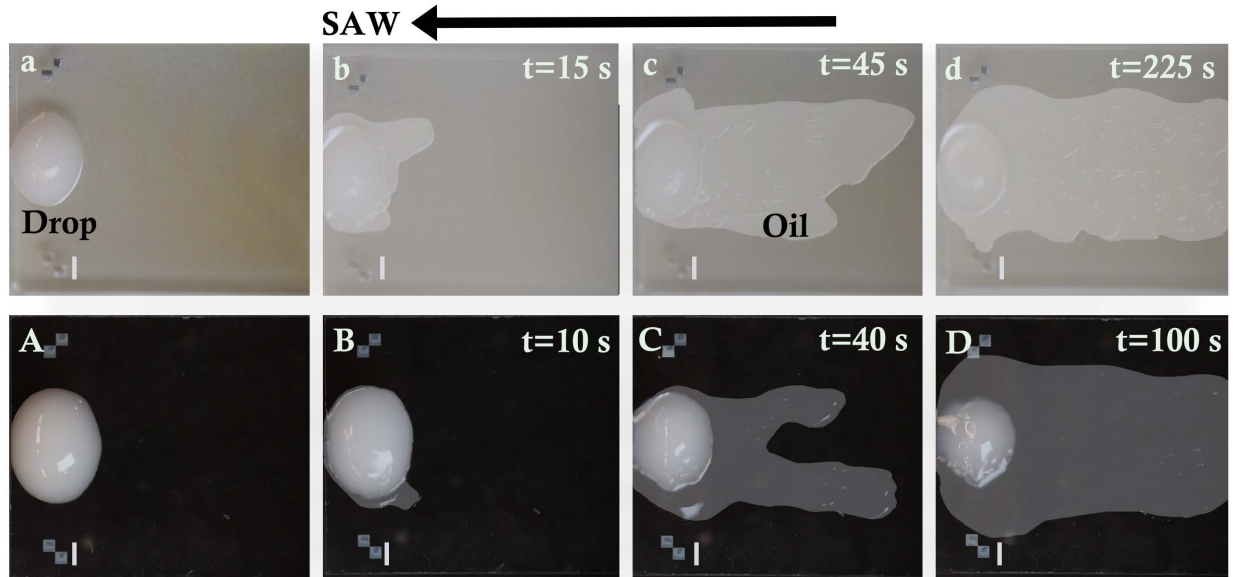


Figure 4: Top view of a $10 \mu\text{l}$ emulsion drop under SAW excitation ($A = 1.5 \text{ nm}$). (a-d) A drop is placed in a humidity cell (85% humidity) and (A-D) a drop is placed under lab ambient conditions (50% humidity). The time $t = 0$ is taken at the moment (t_w) at which we observe the presence of transparent oil at the circumference of the drop; in (a) $t_w = 465 \text{ s}$ and in (A) $t_w = 170 \text{ s}$. We observe, both when using humidity call and under lab conditions, that the oil films leave the drop and spread over the solid substrate in the direction opposite the path of the SAW (see the arrow that illustrates the direction of the SAW above the images), but at different times. The white scale line is 1 mm long. The difference in shade between the two experiments results from the presence of a transparent solid substrate between the drop in the humidity cell and the camera in (a-d), and the slightly non-spherical shape of the drop is due to the pinning of the drop by the edge of the actuator on the left hand side of the images. See SI for additional figures and videos.

half the ultrasound wave leakage off the SAW. Figure 6 shows a side view image of our laser interferometry experiment,²¹⁻²³ comprising a red laser source, mounted on a protractor to identify the angle of the laser relative to the oil film, and a camera mounted at the opposite angle to the laser source. The interaction of the laser with a nearly flat and smooth oil film results in light fringes of equal chromatic order (FECO). The light fringes appear as dark and bright areas that map spatial variations in film thickness. We estimate the height difference associated with a path along the surface of the film by crossing from bright to dark and then

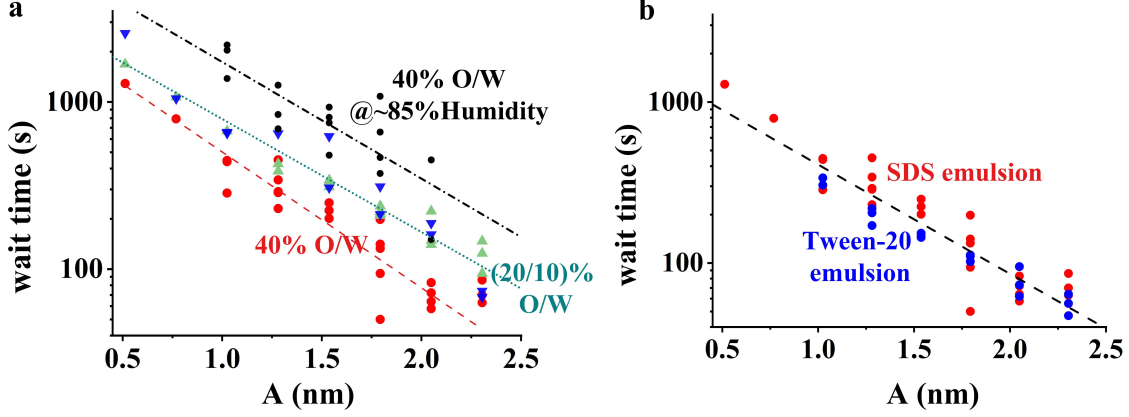


Figure 5: SAW intensity (A) versus the waiting time, t_w , for the appearance of oil films, for (a) different initial oil concentrations and ambient humidity levels, and (b) different surfactants.

back to bright fringes or vice versa, i.e., along one period of fringes, using the expression

$$\Delta h = \lambda_0 / (2n_3 \cos(\theta_3)), \text{ where } \theta_3 = \sin^{-1}(\sin(\theta_1)/n_3), \quad (1)$$

with λ_0 the wavelength of the incident light, n_3 the refractive index of the oil, and θ_1 the angle between the laser beam and the normal to the free surface of the oil film.

Figure 7 shows an example of an oil film extracted from a sessile emulsion drop (view from above). Here, the emulsion drop is located at the bottom left of the images in the top panel, outside the red spot of the laser, which is aimed at an oil ‘finger’ (see Fig. 2) emerging from the drop. The oil film that leaves the drop appears in the form of a bright-red and dark pattern. In the presence of SAW, we do not observe the usual regular light fringe (FECO) patterns that portray thickness variations along a film of smooth surface. Rather, the patterns, shown in Fig. 7(A), suggest that in the presence of SAW the oil films undergo abrupt spatial periodic changes in thickness, shown as cell-like spatial variations in bright and dark patterns (see A1, the zoom-in of Part A of Fig. 7). The appearance of these cell-like thickness variations in the presence of the laser beam suggests spatial variations in film thickness that correspond to 1/4 to 1/2 of the 635 nm laser beam wavelength, i.e., thickness variations of approximately 0.15 to 0.3 μm . These thickness variations appear to

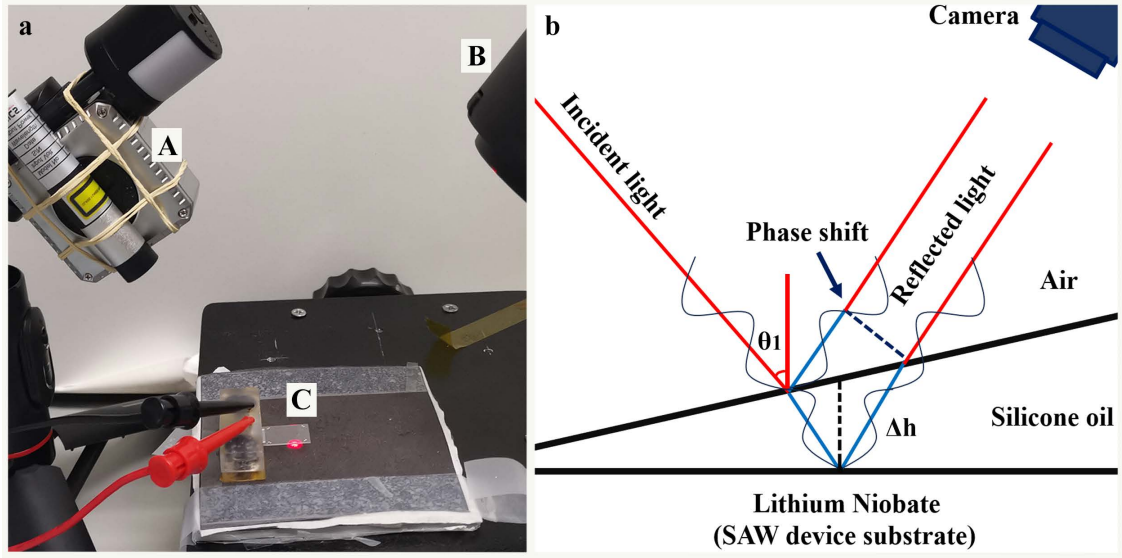


Figure 6: (a) A side view image of our laser interferometry experiment, where the components marked by ‘A’, ‘B’, and ‘C’ are a digital protractor to monitor light angle emission with respect to the target surface, the position of the measured oil film, and a camera mounted at the opposite angle to the protractor, respectively. In (b), we illustrate the laser path in air and the oil film.

be a consequence of capillary/acoustic instability at the free film surface, which introduces sub-micron spatially periodic deformations.

The cell-like patterns hinder the formation of ordered FECO patterns, and hence the measurement of the film thickness. To measure the film thickness, we turn the SAW off. Figure 7(B), taken 1 second from the moment the SAW is turned off, shows that the film surface is sufficiently smooth at this time to support a well-ordered FECO pattern that allows for film thickness measurement. We find that the oil film is comprised of thick and thin step-like regions, illustrated schematically in Fig. 7(C). The thick parts of the film show the cell-like pattern in the presence of SAW. The thin parts do not support the cell-like pattern, showing well-ordered FECO patterns.

The thin parts of the oil film appear to be wetting oil layers of typical thickness $1\text{-}3\ \mu\text{m}$; see Methods for more details. The thicker part of the film is measured to be approximately $25\ \mu\text{m}$ thick, between $1/4$ to $1/2$ of the ultrasound leakage wavelength of $75\ \mu\text{m}$ (the ultrasound is of 20 MHz frequency and propagates at a phase velocity of approximately 1,500 m/s in oil).

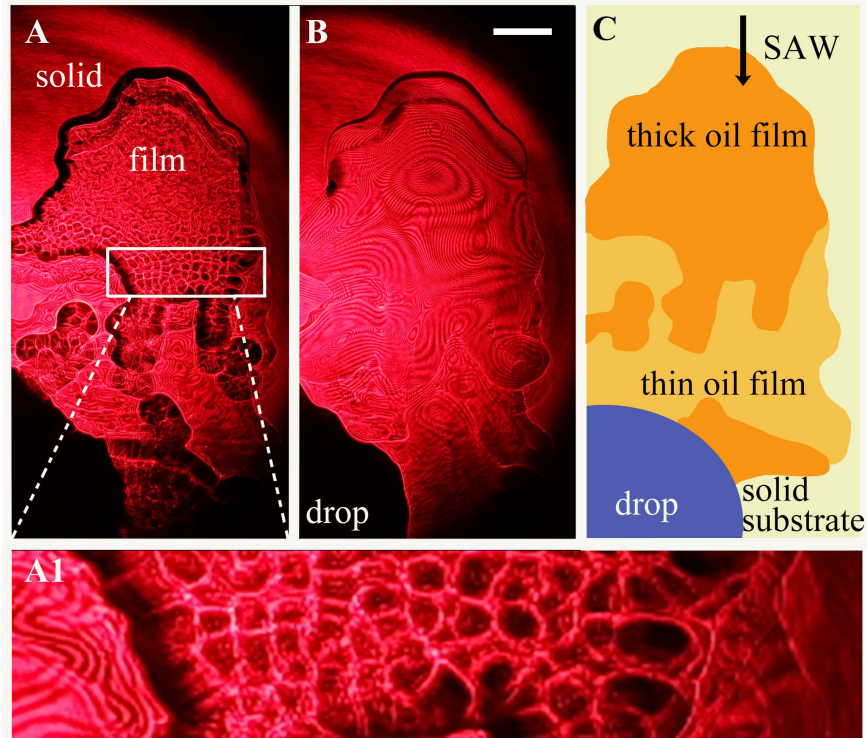


Figure 7: Laser interferometry FECO (fringes of equal chromatic order) patterns on an oil film extracted from an emulsion drop (dark shadow at the left bottom corner) under SAW of amplitude $A = 1.5$ nm, where we show (A) the cell-like pattern while the SAW is active (image A1 shows zoom-in of the region bounded by the white rectangle in (A)), and (B) the orderly FECO patterns 1 s from the moment the SAW was turned off (the white scale bar is 0.5 mm long). Part (C) shows a sketch of (A) to help the interpretation of the results; the darker yellow color indicates a thicker oil film.

Hence, our observations are consistent with the film thickness anticipated in acoustowetting, suggesting that this is the mechanism that drags the thick oil films out of emulsion drops in the presence of the SAW.

Variations in oil content in the emulsion drops

Spatial variations

One of the mechanisms that appear to contribute to the rate at which oil films leave the emulsion drop is the spatial distribution of oil emulsion droplets in the sessile drop under SAW excitation. Studies of the acoustowetting phenomenon^{11,12,15,16} show that in single-

phase systems, i.e., oil or water/surfactant solutions, films of liquid leave reservoirs of the pure liquids en-masse, in the direction opposite to the SAW propagation. However, in Fig. 2, we see that when the reservoir is an emulsion rather than a pure phase, the oil phase leaves the emulsion drop transverse to the path of the SAW in the form of oil fingers. Once the oil fingers are sufficiently far away from the drop, they start spreading in the direction opposite to the SAW propagation, as expected. This initial motion of the oil fingers transverse to the path of the SAW suggests depletion in oil content (inhomogeneous distribution of oil emulsion droplets) in the part of the drop closest to the IDT, as we discuss next.

To measure the spatial distribution of oil emulsion droplets, we use emulsions characterized by different oil content and vary the intensity level of SAW excitation. We identify spatial variations in the concentration of the oil phase in the emulsion drop by monitoring the diffraction of white light therein. Using the principles of the Beer-Lambert law,²⁴ we estimate the emulsion content during our oil extraction experiment using variations in the brightness level of the measured drop: as light passes through the emulsion, it is scattered by the oil droplets therein. Light scatter increases with the concentration of oil emulsion droplets and with the light path length as it travels through the drop.

Figure 8 shows that the SAW renders the front of the drop (toward the source of the SAW) transparent (appearing black due to the color of the substrate below the emulsion drop), and the back of the drop opaque white. Contributions of the oil film (that forms on the drop) to light diffraction are assumed to be small. Thus, Fig. 8 suggests that the SAW ‘pushes’ the oil droplets to the back of the sessile emulsion drop. The transparent (dark) areas of the sessile drops indicate local areas of low oil concentration, where light undergoes weak diffraction. The non-transparent (bright) areas of the drops contain larger concentrations of oil droplets, where light undergoes appreciable diffraction. We note that this is only a rough map of oil concentration since both the curvature of the free surface, and the drop thickness, which also contribute to the extent of light diffraction, vary from location to location. Still, while our analysis gives only qualitative insight into the spatial

distribution of the oil emulsion droplets in our experiments in real-time, it is sufficient to demonstrate the spatial nonuniformity of the oil droplet content.

In an effort to make the spatial nonuniformity of the oil droplet content in the emulsion drops easier to grasp, we coarse-grain the emulsion drop images to binary (white and black) color maps to represent areas of excess and depleted oil droplets therein. We commence this analysis by converting each drop image to a gray-scale scheme, where each pixel is represented by a range of numerical values between 0 and 1. Bright parts of the emulsion drops, represented by gray-scale numerical pixel values of 0.5 or larger indicate excess oil droplet concentration in the emulsion drop (relative to its initial oil droplet content) and are assigned the binary numerical value 1. Dark parts of the emulsion drops, represented by gray-scale numerical pixel values below 0.5, indicate areas of depleted oil droplet concentration in the emulsion drop and are assigned the binary value 0. We plot the ratio, Θ , of the emulsion drop bright area to the total area of the emulsion drop in Fig. 9.

An emulsion drop containing a uniform oil droplet concentration throughout its volume gives $\Theta = 1$, while a smaller Θ -value reflects that a portion of the drop volume is oil-depleted. We find that (1) the Θ -value is significantly smaller under SAW excitation when compared to the uniform distribution ($\Theta = 1$), and (2) within the measurement uncertainty (deviation between 2 to 3 repetitions of the measurements), Θ is largely independent of the specific SAW intensity. Moreover, the value of Θ in the presence of SAW is sensitive to the overall concentration of oil in the drop. It decreases when the initial oil content is increased, as may be seen by comparing Figs. 9(a) (lower oil concentrations) and (b) (higher oil concentrations); note the different vertical scales on the two plots. The fact that the SAW pushes the emulsion oil droplets along its path is a well-known phenomenon that originates from the radiation pressure the SAW inflicts on the emulsion droplets, see, e.g., studies by King²⁵, Shilton et al.²⁶, Li et al.²⁷, Rogers et al.²⁸.

To conclude, as a consequence of SAW pushing the oil droplets back within the emulsion drop, the oil leaves the drop from the sides, where the presence of increased oil content serves

as a reservoir.

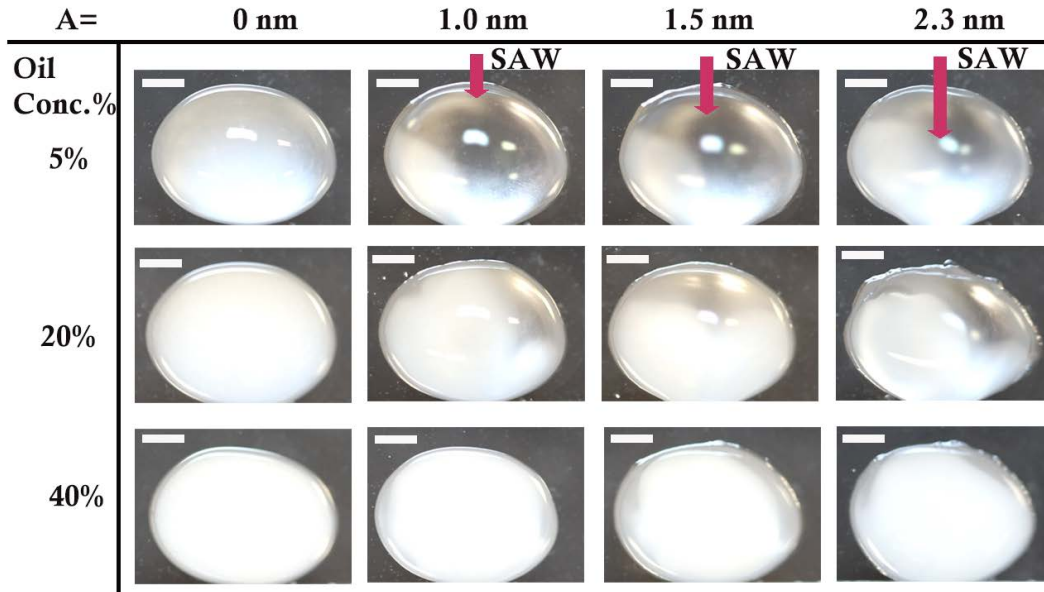


Figure 8: Variations in SAW amplitude (A) and initial oil content in our sessile emulsion drops result in different spatial distributions of oil content under SAW excitation, indicated by transparent (dark) and non-transparent (bright) portions of the drop, which contain small and large concentrations of oil droplets, respectively. In this experiment, the size of the oil droplets was measured to be $4.7 \pm 0.5 \mu\text{m}$. The length of the scalebar in the images is 1 mm. See movies 4 and 5 in the SI as examples of the experiments.

Temporal variations

To obtain a quantitative measurement of the oil content in the emulsion drops under SAW excitation, we monitor time variations in the diffraction of white light from above over a small area of $0.5 \times 0.5 \text{ mm}^2$ about the drop apex. In this region the drop surface curvature is small, and it is easy to identify variations in the local drop thickness, which is just the local path of light through the drop. The measurement is conducted by monitoring the level of light diffraction between the center (apex) of the drops and the solid substrate below, along a light path of length $d(t)$ (twice the height of the drop's apex), serving as a proxy for the concentration of oil droplets under the apex of the drop. We further measure the time variations of the drop height to identify the small variations in the magnitude of $d(t)$

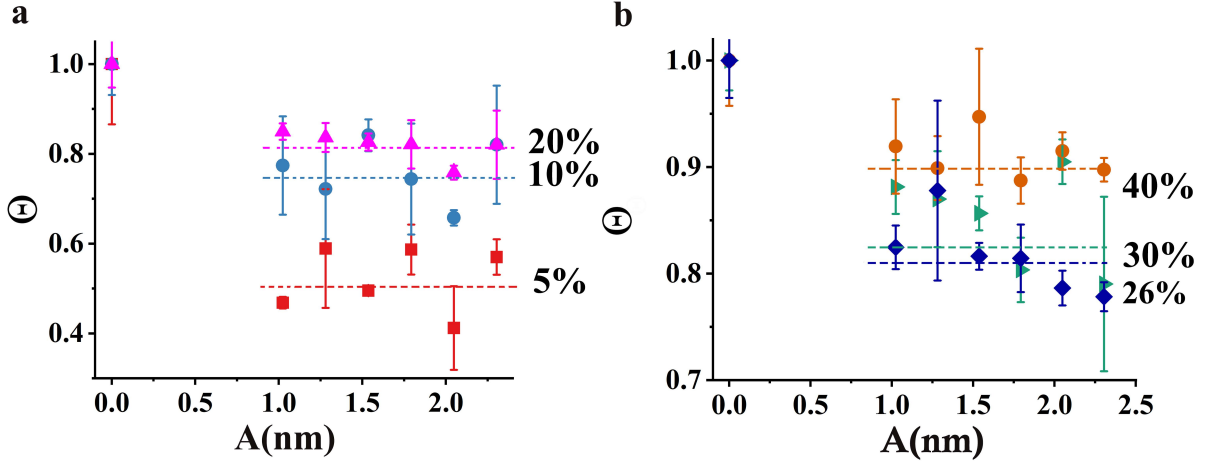


Figure 9: Variations of Θ (the ratio between the area of the drop where oil concentration is in excess, to the full area of the drop, when viewed from above) with SAW amplitude A . The dashed lines represent the average value of Θ for three different fixed values of the oil concentration (the corresponding experimental data points are matched by color and symbol). Part (a) shows results for emulsions with low oil concentrations; part (b) for emulsions with higher oil concentrations (note the different vertical scales on (a) and (b)).

during the measurement. Assuming that changes in the size of the emulsion oil droplets during the experiment are minor and that contributions to light diffraction from the oil film that appears at the free surface are small, we convert our results to oil concentration using a Beer-Lambert-type expression derived from first principles²⁹ (see Methods for further details),

$$-\log_{10}(1 - \hat{I}(t)/\hat{I}_0) = (\varepsilon c(t) + b)d(t), \quad (2)$$

where $\hat{I}(t)$ and \hat{I}_0 are the time-dependent level of the temporal gray shade of the drop on a calibrated gray scale and the initial gray shade of the drop, respectively. As noted, $d(t)$ is the time-dependent light path length through the drop, ε is the light absorbance coefficient, b is a calibration parameter accounting for light reflection from the substrate below the drop, and $c(t)$ is the concentration of oil droplets in the emulsion. We stop the experiment when the drop loses approximately 20% of its initial 10 μl volume. Beyond this point, the three-phase contact line tends to move, and the shape of the sessile drop deforms, reducing the measurement accuracy. The measurement is conducted in lab ambient conditions; see

further details in Methods and calibration details in SI.

Figure 10 shows time variations of the oil droplet concentration, $c(t)$, obtained using equation (2) with appropriate values for $\hat{I}(t)$, \hat{I}_0 , $d(t)$ measured from the experiment, with ϵ , b obtained using calibration (see Methods). We measure the evolution of the oil content under the drop apex for three different initial oil concentrations. In the absence of SAW, we observe that the oil concentration reduces over time for all considered initial oil concentrations. This is attributed to the transformation of oil droplets in the emulsion to an oil film at the emulsion drop surface, a process enhanced by the evaporation of water.^{19,20} Since this oil film diffracts light ineffectively compared to the oil droplets in the emulsion, the level of light diffraction is reduced as time progresses.

Once the SAW is applied, the results become more elaborate, with the trend depending on the overall oil concentration. In the case of 50% initial oil concentration, we observe from Fig. 10 that the temporal oil content near the drop apex reduces over time in the presence of SAW. In the case of the initial 30% oil content, the temporal oil content increases over time, and in the case of an initial 40% oil content, the oil content appears to fluctuate over time. These opposing trends in the content of oil near the drop apex are attributed to three factors: (1) the enhanced rate by which oil leaves the drop under SAW excitation,^{11,12,15,16} reducing the concentration of oil in the drop; (2) the rate at which water leaves the drop by evaporation,^{19,20} which is also enhanced when increasing the intensity of the SAW; see SI for further details about SAW-enhanced water evaporation; and (3) the spatial variation of oil droplet content due to the SAW ‘pushing’ the oil droplets to the back of the drop - this effect is enhanced when reducing the concentration of oil therein and increasing the intensity of the SAW.

One interpretation of the results is that a larger initial oil concentration (Fig. 10a) increases the rate at which oil leaves the drop. An initial oil droplet concentration of 40% appears to introduce a threshold, specific to the conditions in our experiment, for the ratio of the rates at which oil and water leave the drop. At this value, both appear to leave the

drop at similar rates, which gives rise to an oil droplet concentration that varies little over time. An initial oil concentration above the 40% threshold results in oil leaving the emulsion drop at a higher rate (leading to negative slope of the data in Fig. 10a), and one below the 40% threshold results in oil leaving the drop at a smaller rate (positive slope of data in Fig. 10b).

This interpretation, however, ignores the internal spatial distribution of oil droplets in the emulsion drop, generated by the SAW, and also that the ratio between the rates at which oil and water leave the drop appears to be determined by the initial oil droplet concentration rather than by its temporal concentration. More research is needed to precisely understand the influence of the interplay between these different mechanisms on the evolution of the oil droplet concentration in the emulsion drop.

Conclusion

We use acoustic stress to extract oil from oil-in-water emulsions by discriminating over the different surface tensions and the different wettability properties of the two phases.³⁰ We employ surface acoustic waves (SAWs) to invoke the *acoustowetting* phenomenon,^{31,32} where a balance between acoustic and capillary stresses support spreading of the oil phase in the direction opposing the SAW. Silicone oil fully wets the solid substrate of the SAW actuator, while water and water/surfactant solutions partially wet the solid substrate, supporting a finite three-phase contact angle of between 30 and 60°, depending on the level of surfactant added. Judicious use of SAW power renders the dynamic wetting of the solid by the oil phase while keeping the water phase at rest.

In our experiments, we subject sessile 10 μl emulsion drops to a 20 MHz-frequency traveling surface acoustic wave (SAW) in a SAW actuator. We observe that the waiting time required for the formation of oil films that leave the emulsion drop may last from tens of seconds to tens of minutes from the commencement of the experiment. The waiting time is

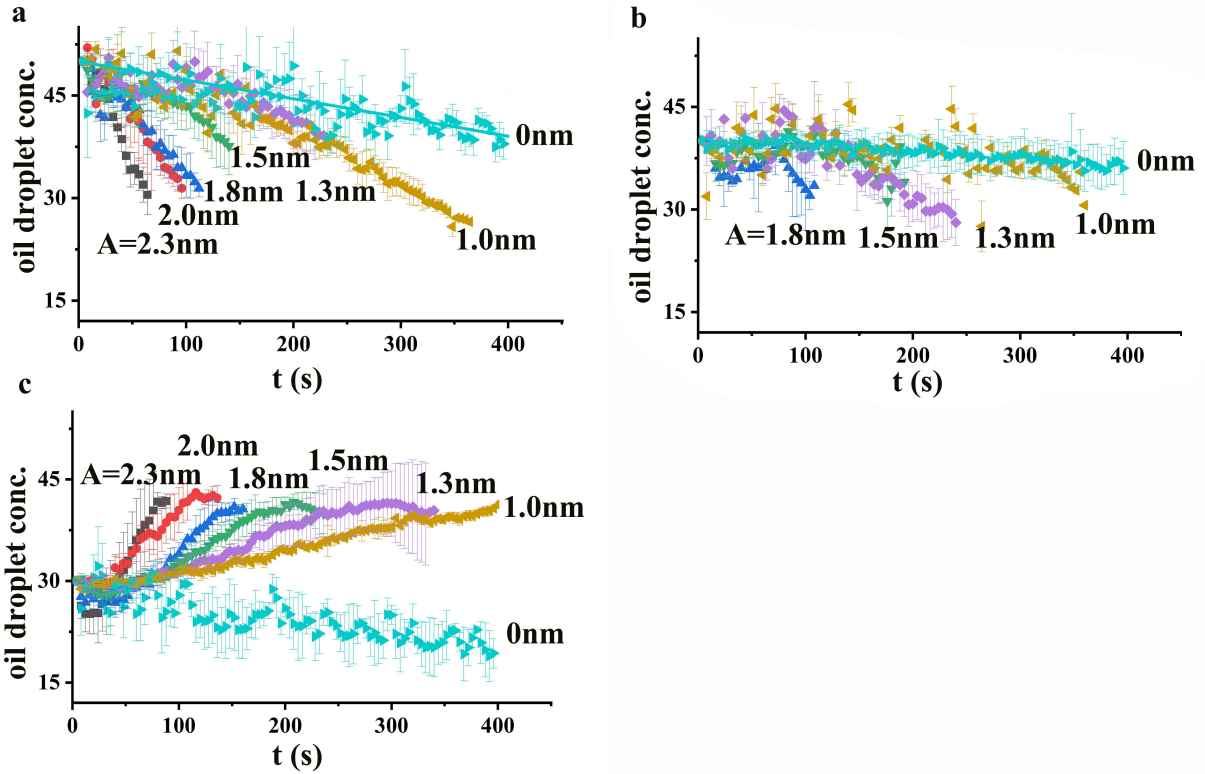


Figure 10: Time (t) variations of oil droplet concentration from the moment SAW was applied to the substrate in different emulsion sessile drops under SAW excitation for initial oil concentration of (a) 50% (b) 40%, and (c) 30%, where the error bars show average deviations in value taken from 2 repetitions of the experiment; we give the corresponding SAW intensity A for each experiment on the graphs. The measurement is taken from above through a square of $0.5 \times 0.5 \text{ mm}^2$ at the apex of the drop, while changes in the drop height are accounted for when converting the level of liquid diffraction to oil droplet concentration; the solid lines are guides to the eye where useful.

reduced when increasing the SAW intensity and increased when ambient humidity is augmented. The resulting acoustic radiation pressure in the drop spatially redistributes the emulsion droplets, reducing their concentration at the front of the drop (the portion of the drop nearest the IDT, the source of the SAW).

The reduced oil concentration at the front of the drop appears to inhibit oil extraction from that part of the emulsion drop due to the local lack of oil droplets therein. Instead, we observe ‘fingers’ of oil films to appear first at the sides of the drop, transverse to the source of the SAW. The oil films initially leave the drop in the direction transverse to the SAW.

At later times, the oil film outside the drop changes direction and spreads in the direction opposite to the SAW propagation. This is a counter-intuitive finding since one expects the oil to leave the drop from the front, facing the source of SAW, similar to the previous studies of acoustowetting. Thus, the physics of extracting a liquid film from a pure liquid reservoir using SAW differs from the physics of extracting a liquid film from a complex liquid, such as the emulsion drops in our experiment. Nonetheless, the oil film appearing at the solid surface is of thickness approximately $25\ \mu\text{m}$, which is between $1/4$ and $1/2$ of the wavelength of the ultrasound that leaks off the SAW into the liquid. This further confirms our claim that the acoustowetting phenomenon is responsible for the low surface energy oil films that leave the emulsion drop and spread over the solid while keeping the high surface tension water phase at rest, at least for the SAW intensity level used in our experiments.

In addition, we observe several types of interfacial instabilities that are likely a result of the competition between acoustic and capillary stresses in the oil films that leave the emulsion drop. The oil initially leaves the drop in the form of ‘fingers’ which later merge into a continuous oil film that develops spatial variations in thickness. The lateral length scale for the variation in film thickness is approximately $0.5\ \text{mm}$ —different from the $200\ \mu\text{m}$ wavelength of the SAW, suggesting that the film thickness variation is not directly related to the SAW wavelength. Moreover, in the presence of SAW, we observe that the thick oil films support a crystal-like cell pattern observed using interferometric measurements. The patterns are characterized by a lateral length scale of tens of microns and are associated with spatially periodic thickness variations of 0.1 to $0.3\ \mu\text{m}$. The variations in film thickness correspond to a quarter of the red laser wavelength that we use for our measurements, and hence are observed during our interferometric measurements. The pattern formation phenomena exist in the presence of SAW and fade away within seconds once the SAW is turned off.

In conclusion, we are encouraged by the potential of using SAW to extract oil from oil/water mixtures by discriminating over their different surface tension and wetting prop-

erties. We highlight the physics underlying this opportunity as well as various phenomena that we observe and that should be resolved to facilitate such a technology.

Methods

Emulsion preparation and characterization

Preparing emulsions, we used 50 cSt silicone oil (Sigma-Aldrich, 50cSt, 378356-250ML) and HPLC water (Macron Fine Chemicals, ChromAR[®]), in addition to Sodium Dodecyl Sulfate, i.e., SDS, (Sigma-Aldrich, GC, 74255-250G) and Tween 20 (Sigma-Aldrich, P1379-100ML) as surfactants. The emulsions were prepared by mixing silicone oil and aqueous surfactant solution (4mM for SDS, 0.5%wt for Tween 20. We commenced the preparation by emulsifying mixtures of oil and water/surfactant solutions (total volume of 50ml) using Rotor-stator mixer (PRO Scientific Inc. Bio-Gen Series PRO 200) for 60 seconds at maximum power. The emulsion droplets were then further reduced in size by sonication, applying 180 seconds of ultrasonic emulsification (Qsonica LLC, Q500) with 30% power output, 5/20 pulse mode. The energy (fixed power & changing time) of mixing/sonication was proportionally reduced based on the volume of liquid. We used Dynamic Light Scattering (DLS) measurement of the emulsions using Zetasizer Ultra (Zetasizer Ultra, Malvern, UK) to measure the size distribution of the oil droplets in the emulsions. The emulsions underwent 100 times dilution using 4 nM SDS solution and where relevant Tween 20 solution to satisfy the dilution requirement of the DLS measurement.

Actuator fabrication and experimental procedure

To fabricate surface acoustic wave (SAW) actuators, we used standard lift-off photolithography to fabricate 24 electrode pairs of 5 nm titanium / 1 μ m aluminum interdigitated electrode (IDT) and bus bars for connection to external electric circuit atop 0.5 mm thick, 128° Y-cut, X-propagating, single-crystal lithium niobate piezoelectric wafer (Roditi International, UK)

wafers. The wafer was subsequently cut to individual 20 MHz-frequency SAW actuators. We power the actuators using a signal generator (ROHDE&SCHWARZ, SMB100A microwave signal generator) and amplifier (Tabor Electronics, model A10160, Israel) and measured the nanometer normal surface displacement amplitude (intensity) of the Rayleigh SAW in the actuators using a scanning laser Doppler vibrometer (MSA-500, Polytech). This measurement further confirmed that the SAWs are traveling waves. Before every experiment, we washed the SAW actuator for 30 s with 4 different solvents in the following order: acetone (AR-b, 99.8%, 67-641, Bio-Lab Ltd.), 2-propanol (AR-b, 99.8%, 67-63-0, Bio-Lab Ltd.), ethanol (CP-p, 96%, 64-17-5, Bio-Lab Ltd.), and water (ChromAR[®] HPLC, Macron Fine Chemicals).

We fix and connect the SAW actuators by pogo-pins (BC201403AD, Interconnect Devices, Inc.) attached to a 3D-printed elastomeric stage (shown in fig. 1(a)) under ambient lab environment ($20 \pm 2^\circ$ Celsius and $50 \pm 5\%$ humidity) and in a humidity chamber ($20 \pm 2^\circ$ Celsius and $85 \pm 5\%$ humidity). To fabricate the humidity chamber shown in fig. 1(c), we employ a commercial glass petri-dish and a plastic cover. We further put a small hole in the plastic cover to connect the SAW actuator to power via electric wires. The wires were attached to the SAW actuator using a conductive silver-epoxy (EPO-TEK[®] H20E, Epoxy Technology, Inc.). Another hole was used to monitor the internal temperature and humidity in the chamber using a dedicated sensor (EARU Electric). Moreover, the experiments are recorded using a camera (EOS R5, Canon) fit with a macro lens (RF 100mm F2.8L MACRO IS USM, Canon). We further employ a light diffuser (a rough plastic surface) between the light source and the experiment to reduce the level of localized concentrated light areas. We capture videos of the experiment using camera Aperture 4.0, Shutter Speed 1/320, and ISO (5000) to reduce the effect of the camera light auto-adjustment.

During the experiment, we place $10 \mu\text{l}$ emulsion drops atop the SAW actuator, far from the electrodes, see Fig. 1. The oil droplets in the emulsion have an average diameter of 230 nm (the diameter of droplets is calculated based on the number of drops in the emulsion),

with oil concentration of 10-50% by volume. The emulsions are stabilized using surfactants (SDS or TWEEN20). The SAW actuator is activated immediately following the placement of a drop. We measure the temperature of the solid surface near the emulsion before and after the activation of SAW. When using the humidity chamber, we waited for 10 minutes from the moment we placed the drop atop the SAW device and closed the chamber, before applying power to the SAW actuator, to stabilize the humidity therein prior to the commencement of the experiment.

Interferometric oil thickness measurements

We generate FECO fringes to estimate the height of the oil film induced by the Surface Acoustic Wave (SAW). For the light interference experiments, we mount a level-1 laser generator (635 nm, LM-6305MR, Lanics) and a camera (EOS R5, Canon) at similar angle with respect to the horizon to observe the FECO patterns induced by the light interference. The angles are monitored using a digital protractor attached to the laser generator. During the measurement, we shine the 635 nm laser at the oil film to result in constructive and destructive light interference patterns (light fringes) at the oil free surface due to the additional optical path traveled by the light reflected from both the oil/air and oil/solid interfaces.

Regarding the uncertainty in our measurement, four independent measurements give less than 3% deviation between the different measured values. The measurements given are taken 1 second after the SAW in the substrate is turned off, following the disappearance of the cell-like interferometric patterns atop the films. To estimate the uncertainty in the measured film thickness due to the 1 second wait, we resort to the thin film equation:³³ accounting for mass and momentum conservation, the long wave approximation of film dynamics, which is governed by capillary stress and viscous dissipation, is given by the film equation $\partial h/\partial t = (\gamma/3\mu)\nabla_s \cdot (h^3\nabla_s\nabla_s^2h)$, where h and t are the local film thickness and time, $\gamma = 20 \times 10^{-3}$ N/m and $\mu = 50 \times 10^{-3}$ Pa·s are the silicone oil film surface tension (against vapor) and

viscosity in our experiment, and ∇_s is a gradient operator along the solid surface. The film thickness scales like its measured value, $h \approx h_{\max} = 25 \mu\text{m}$. The gradient operation scales like the inverse of the characteristic lateral length scale of the film, i.e., $\nabla_s \approx 1/l_{\text{film}} = 1 \text{ mm}^{-1}$. Hence, the scale for the rate of change in film thickness is given by $\partial h/\partial t \approx (\gamma/\mu) \times h_{\max}^4/l_{\text{film}}^4 \approx 10^{-1} \mu\text{m/s}$. The characteristic change in local film thickness within 1 second is then $0.1 \mu\text{m}$. Hence the uncertainty in the maximum film thickness due to the 1 second wait in our experiment is $0.1 \mu\text{m}/25 \mu\text{m} \approx 0.4\%$. Therefore, the overall uncertainty in the maximum measured film thickness is approximately $3.4\% \approx 4\%$, when accounting for both variability between measurements, and the relaxation of the oil film in the 1 second time wait from the moment we turn off the SAW and until we take the measurement.

The change in local film thickness during the one second waiting time is of similar magnitude to the characteristic difference between bright and dark interferometric light patterns of approximately $0.16 \mu\text{m}$ (a quarter of the laser wavelength). Hence, the micro-cell pattern appearing on top of the macro-film structure as an interferometric pattern in the presence of the SAW is associated with a local film thickness variations of a similar magnitude.

Measuring oil content using a Beer-Lambert-like rule

The simple form of the Bouguer-Beer-Lambert Law gives the equation

$$-\log_{10}(I/I_0) = \varepsilon cd, \quad (3)$$

where I_0 is the original light intensity, I is the light intensity after traveling through a media that contains a molar concentration of objects, c , that are of molar absorption coefficient ε , assumed constant throughout each experiment, and d is the path length of the light in the medium. The right hand side of the equation is the light absorbance of the medium, given by εcd . Moreover, in each experiment, we calibrate (scale) the value of light intensity I and I_0 against variations in ambient light by placing the same white paper next to the experi-

ment. As a precaution, the values of I and I_0 are normalized against (divided by) the color intensity of the paper in each experiment, so that we are able to compare between different experiments. The corresponding normalized values are denoted by \hat{I} and \hat{I}_0 , respectively.

The brightness that we observe on the emulsion drop is a result of light scatter by the emulsion. The emulsion drop becomes continuously darker (and more transparent) when the emulsion concentration is reduced and when the thickness (height) of the drop is reduced. Monitoring the change in the light intensity (brightness) of the emulsion over time, $\hat{I} = \hat{I}_0 - \hat{I}(t)$, we rewrite (3) in the form

$$-\log_{10}((\hat{I}_0 - \hat{I}(t))/\hat{I}_0) = -\log_{10}(1 - \hat{I}(t)/\hat{I}_0) = (\varepsilon c(t) + b)d(t), \quad (4)$$

where we added the constant b to account for light reflection from the substrate below the drop. We find the constants ε and b using a calibration curve constructed from measuring a series of emulsion drops of known oil concentration. The magnitude of $d(t)$ is twice the drop maximum thickness (height) and is measured over time, t , throughout each experiment in tandem with the light intensity measurement. Following the experiment, we convert the measured light intensity at the apex of the drop to an approximation of the time-dependent concentration of oil droplets therein, $c(t)$. Moreover, since in our experiments the SAW renders a spatial redistribution of oil droplets inside the bulk emulsion drops, the measured quantity $c(t)$ is an approximation of the average concentration of emulsion droplets in the drops.

Acknowledgement

This work was supported by US-Israel Binational Science Foundation (BSF) under grant No. 2020174 and by the donors of ACS Petroleum Research Fund under Grant PRF# 62062-ND9. J.M.M. is grateful to the Spanish Ministerio de Universidades for a predoctoral fellowship No. FPU2021-01334. J.A.D. acknowledges support from Consejo Nacional de In-

investigaciones Científicas y Técnicas (CONICET, Argentina) with Grant PIP 02114-CO/2021 and Agencia Nacional de Promoción Científica y Tecnológica (ANPCyT, Argentina) with Grant PICT 02119/2020.

Supporting Information Available

A listing of the contents of each file supplied as Supporting Information:

The following files are available:

- Movie 1. Top view video of an experiment in ambient lab conditions. Oil concentration: 40%, SAW amplitude: $A = 1.25$ nm.
- Movie 2. Side view of a similar experiment. Oil concentration: 40%, SAW amplitude: $A = 1.75$ nm.
- Movie 3. Top view of a laser diffraction experiment. Oil concentration: 40%, SAW amplitude: $A = 1.75$ nm.
- Movie 4. Top view of oil droplet response to SAW in the emulsion drop for different drop oil content and SAW amplitudes.
- Movie 5. Top view of oil droplet response to SAW in the emulsion drop. Oil concentration: 40%, SAW amplitude: $A = 1.00$ nm.
- A Supplementary Information document that includes emulsion properties; measured calibration curve between applied voltage and the SAW displacement amplitude, A ; Code for the analysis of the light diffraction level in the emulsion drop; and details for the interferometry measurement of the oil film thickness.

References

- (1) Daughton, C. Cradle-to-cradle stewardship of drugs for minimizing their environmental disposition while promoting human health. I. Rationale for and avenues toward a green pharmacy. *Environ. Health Perspect.* **2003**, *111*, 757–774.
- (2) Osborn, S. G.; Vengosh, A.; Warner, N. R.; Jackson, R. B. Methane contamination of drinking water accompanying gas-well drilling and hydraulic fracturing. *Proc. Natl. Acad. Sci. U. S. A.* **2011**, *108*, 8172–8176.
- (3) Vidic, R. D.; Brantley, S. L.; Vandenbossche, J. M.; Yoxtheimer, D.; Abad, J. D. Impact of Shale Gas Development on Regional Water Quality. *Science* **2013**, *340*.
- (4) Nacheva, P. M.; Camperos, E. R.; Yoval, L. S. Treatment of petroleum production wastewater for reuse in secondary oil recovery. *Water Sci. Technol.* **2008**, *57*, 875–882.
- (5) Lefebvre, O.; Moletta, R. Treatment of organic pollution in industrial saline wastewater: A literature review. *Water Res.* **2006**, *40*, 3671–3682.
- (6) Westhoek, H.; Lesschen, J. P.; Rood, T.; Wagner, S.; De Marco, A.; Murphy-Bokern, D.; Leip, A.; van Grinsven, H.; Sutton, M. A.; Oenema, O. Food choices, health and environment: Effects of cutting Europe’s and dairy intake. *Global environ. chang.* **2014**, *26*, 196–205.
- (7) Hoekstra, A. Y.; Mekonnen, M. M. The water footprint of humanity. *Proc. Natl. Acad. Sci. U. S. A.* **2012**, *109*, 3232–3237.
- (8) Gorak, A.; Sorensen, E. *Distillation: Fundamentals and Principles*; Elsevier, 2014.
- (9) Zouboulis, A.; Avranas, A. Treatment of oil-in-water emulsions by coagulation and dissolved-air flotation. *Colloids Surf A* **2000**, *172*, 153–161.

- (10) Ahmad, A.; Ismail, S.; Bhatia, S. Optimization of coagulation-flocculation process for palm oil mill effluent using response surface methodology. *Environ. Sci. Technol* **2005**, *39*, 2828–2834.
- (11) Rezk, A. R.; Manor, O.; Friend, J. R.; Yeo, L. Y. Unique fingering instabilities and soliton-like wave propagation in thin acoustowetting films. *Nat. Commun.* **2012**, *3*, 1167–1173.
- (12) Rezk, A. R.; Manor, O.; Yeo, L. Y.; Friend, J. R. Double flow reversal in thin liquid films driven by megahertz-order surface vibration. *Proc. Royal Soc. A* **2014**, *470*, 20130765.
- (13) Manor, O.; Rezk, A. R.; Friend, J. R.; Yeo, L. Y. Dynamics of liquid films exposed to high-frequency surface vibration. *Phys. Rev. E* **2015**, *91*, 053015.
- (14) Collins, D. J.; Manor, O.; Winkler, A.; Schmidt, H.; Friend, J. R.; Yeo, L. Y. Atomization off thin water films generated by high-frequency substrate wave vibrations. *Phys. Rev. E* **2012**, *86*, 056312.
- (15) Altshuler, G.; Manor, O. Spreading dynamics of a partially wetting water film atop a MHz substrate vibration. *Phys. Fluids* **2015**, *27*, 102103.
- (16) Altshuler, G.; Manor, O. Free films of a partially wetting liquid under the influence of a propagating MHz surface acoustic wave. *Phys. Fluids* **2016**, *28*, 072102.
- (17) Horesh, A.; Khaikin, D.; Karnilaw, M.; Zigelman, A.; Manor, O. Acoustogravitational balance in climbing films. *Phys. Rev. Fluids* **2019**, *4*, 022001(R).
- (18) Tadros, T. F. Emulsion science and technology: a general introduction. *Emulsion science and technology* **2009**, *1*, 43.
- (19) Bouchama, F.; Estramil, G.; Autin, A.; Koper, G. Film formation from concentrated emulsions studied by simultaneous conductometry and gravimetry. *Colloids and Surfaces A: Physicochemical and Engineering Aspects* **2002**, *210*, 129–135.

- (20) Aranberri, I.; Binks, B.; Clint, J.; Fletcher, P. Evaporation rates of water from concentrated oil-in-water emulsions. *Langmuir* **2004**, *20*, 2069–2074.
- (21) Freeman, M. H. *Optics*; Butterworth-Heinemann, 1990.
- (22) Jenkins, F. A.; White, H. E. Fundamentals of optics. *Indian Journal of Physics* **1957**, *25*, 265–266.
- (23) White, J. C. *High-frame-rate oil film interferometry*; California Polytechnic State University, PhD thesis 2011.
- (24) McClements, D. J. Theoretical prediction of emulsion color. *Advances in colloid and interface science* **2002**, *97*, 63–89.
- (25) King, L. V. On the Acoustic Radiation Pressure on Spheres. *Proceedings of the Royal Society of London. Series A, Mathematical and Physical Sciences* **1934**, *147*, 212–240.
- (26) Shilton, R.; Tan, M. K.; Yeo, L. Y.; Friend, J. R. Particle concentration and mixing in microdrops driven by focused surface acoustic waves. *Journal of Applied Physics* **2008**, *104*.
- (27) Li, H.; Friend, J. R.; Yeo, L. Y. Microfluidic Colloidal Island Formation and Erasure Induced by Surface Acoustic Wave Radiation. *Phys. Rev. Lett.* **2008**, *101*, 084502.
- (28) Rogers, P. R.; Friend, J. R.; Yeo, L. Y. Exploitation of surface acoustic waves to drive size-dependent microparticle concentration within a droplet. *Lab Chip* **2010**, *10*, 2979.
- (29) Swinehart, D. F. The Beer-Lambert law. *Journal of chemical education* **1962**, *39*, 333.
- (30) Xue, Z.; Cao, Y.; Liu, N.; Feng, L.; Jiang, L. Special wettable materials for oil/water separation. *Journal of Materials Chemistry A* **2014**, *2*, 2445–2460.

- (31) Rezk, A. R.; Manor, O.; Yeo, L. Y.; Friend, J. R. Double flow reversal in thin liquid films driven by megahertz-order surface vibration. *Proceedings of the Royal Society A: Mathematical, Physical and Engineering Sciences* **2014**, *470*, 20130765.
- (32) Rezk, A. R.; Manor, O.; Friend, J. R.; Yeo, L. Y. Unique fingering instabilities and soliton-like wave propagation in thin acoustowetting films. *Nature communications* **2012**, *3*, 1167.
- (33) Leal, L. G. *Advanced Transport Phenomena: Fluid Mechanics and Convective Transport Processes*, 1st ed.; Cambridge University Press, 2007.